Projectile ionization in fast heavy-ion–atom collisions

D. Schneider
Physics Division, Argonne National Laboratory, Argonne, Illinois 60439

M. Prost, N. Stolterfoht, G. Nolte, and R. Du Bois*
Bereich Kern- und Strahlenphysik, Hahn-Meitner-Institut für Kernforschung Berlin GmbH, Postfach 390128, D-1000 Berlin 39, West Germany

(Received 16 March 1983)

Electron emission following the ionization of projectile ions has been investigated systematically in collisions with Ne^{q+} and Ar^{q+} ions at several hundred MeV incident on different target gases. The projectile electrons are concentrated within one maximum, the electron-loss peak (ELP). The variation of the shape and intensity of the ELP with the projectile energy, its charge state, the observation angle, and the target gas has been measured. Theoretical predictions which are based on the binary-encounter approximation show, in general, good agreement with the experimental data. The contributions of the different subshells to the ELP are deduced. It is shown that electronic screening of the target nucleus plays an important role in the ionization process of the projectile ions.

I. INTRODUCTION

Electron emission following projectile ionization in ion-atom collisions has been observed in secondary-electron spectra first by Schowengerdt *et al.*[1] and by Wilson and Toburen.[2] Wilson and Toburen[2] have measured angular and energy distributions of electrons ejected in 0.6–1.5-MeV $H_2^+ + H_2$ collisions. They have shown that in the laboratory frame projectile electrons form a significant maximum in the secondary-electron spectrum at an electron energy which corresponds to an electron velocity equal to the projectile velocity. The electrons which are due to the projectile ionization are, in general, superimposed on a continuous background of electrons due to the target ionization. This background can be subtracted and the peak due to the electrons lost from the projectile, the electron-loss peak (ELP), can be investigated separately from the target ionization. The electron loss is due to ionization of the projectile in the screened Coulomb field of the target. The ionization of a heavy-ion projectile and that of the target atom is the same. Thus the electron spectra for symmetric collisions are expected to be equal in the rest frames of the colliding particles. However, considerably different energies are found for target and projectile electrons as they are simultaneously observed in one system of reference, the laboratory frame. Wilson and Toburen[2] deduced experimental cross sections for the ELP at different observation angles and found good agreement with elastic scattering cross sections for electrons incident at velocities equal to the projectile velocity. The agreement gave some first insight into the electron-loss process.

The electron-loss process has since then been investigated in more complex systems by Burch *et al.*[3] using O^{q+} projectiles at tandem energies. The angular dependence of the ELP for such systems has been investigated by Stolterfoht *et al.*[4] Recently, cusp profiles for electron-loss peaks have been investigated near 0° observation angles in collisions with C^{q+}, O^{q+}, and Si^{q+} projectiles traversing He, Ne, and Ar targets.[5] Theoretical work concerning the projectile-electron loss has been performed by Drepper and Briggs,[6] Briggs and Day,[7] and Jakubassa.[8]

We report results from a systematic investigation of projectile-electron loss from fast heavy-ion–atom collisions. Projectile ions, Ne^{q+} and Ar^{q+}, ranging in energy from 3–14.5 MeV/amu were used. The relative intensity of the electron-loss peak has been studied as a function of electron-observation angle, and for a variety of target gases (Ne, Ar, Kr, and Xe) and projectile charge states q.

In Sec. II a general description of the process leading to the emission of projectile electrons is given. In Sec. III the experimental procedure for the measurement of projectile electrons and the analysis of the electron-loss peaks is described. In Sec. IV the experimental results are given and discussed in comparison with calculated ELP's. Atomic units are used throughout this work.

II. THEORETICAL METHOD

As pointed out by Wilson and Toburen[2] the electrons of the incident particle can be considered as a merged beam of electrons traveling with the velocity $\vec{v}_p$ of the incident ions.[9,10] The velocity distribution $f(\vec{v}'_b)$ of the electron which results from their binding to the projectile is taken into account by adding the velocity $\vec{v}'_b$ to $\vec{v}_p$. Thus, electrons with velocity $\vec{v}_b = \vec{v}_p + \vec{v}'_b$ are considered to scatter elastically off the target atom which is represented by a screened Coulomb potential. The energy of the ejected electrons is equal to the incident energy $v_b^2/2$. Hence, it follows that

$$E = \tfrac{1}{2}v_b^2 = \tfrac{1}{2}(v_p^2 + v_b'^2 + 2v_p v'_b \cos\theta') , \tag{1}$$

where θ' is the angle between $\vec{v}_p$ and $\vec{v}'_b$. The mean energy is given by $\bar{E} \sim v_p^2/2$ for $v_p \gg v'_b$. The mean energy of the ELP is equal to the projectile energy divided by the projectile-electron mass ratio. The width of the ELP is primarily determined by the variation of $2v_p\vec{v}'_b\cos\theta$. The velocity v'_b for each subshell is centered around the mean value $\bar{v}'_b$. As θ' varies from 0° to 180° the full width at half maximum (FWHM) of the ELP is obtained approximately by[9]

$$\Delta E = v_p \bar{v}'_b . \tag{2}$$

The formula (1) infers that an increase in projectile velocity v_p amplifies structures in the wave function by projecting the velocity distribution $f(\vec{v}'_b)$ of the different bound projectile electrons on a larger velocity scale. It will be shown further below that structures in the wave function for a specific ionic state of the projectile is projected on the scale of several hundred eV in the laboratory frame.

Drepper and Briggs[6] suggested first calculating the projectile ionization in the rest frame of the projectile and then performing a frame tranformation into the laboratory system. This formalism has a relatively simple form, if the velocity $\vec{v}_p$ of the projectile before the collision is the same as after the collision. This condition is fulfilled for the collision systems investigated here. Thus the double-differential cross section (DDCS) for the emission of an electron in the laboratory frame can be obtained from the DDCS in the projectile frame by

$$\frac{d^2\sigma}{dE\,d\Omega}=\frac{v_b}{v'_b}\frac{d^2\sigma}{dE'd\Omega'} . \tag{3}$$

The DDCS in the projectile frame can be calculated with the use of the binary-encounter approximation (BEA) as formulated by Bonson and Vriens.[11] The DDCS for ejection of projectile electrons is obtained from the elastic scattering cross section folded with the velocity distribution $f(\vec{v}'_b)$ and integrated over $\vec{v}'_b$. The cross section is given as

$$\frac{d^2\sigma}{dE'd\Omega'}=\int_{v'_{\min}}^{\infty} d\vec{v}'_b f(\vec{v}'_b)\sigma(\vec{v}_p,\vec{v}'_b) , \tag{4}$$

$d^2\sigma/dE'd\Omega'$ is the double-differential cross section for the emission of an electron with orbital velocities $\vec{v}'_b$ into an energy interval dE' and into a solid angle $d\Omega'$ by the pure Coulomb potential of the target nucleus. The minimum velocity $v'_{\min}$ is determined from the minimum energy transfer, i.e., binding energy. The velocity distribution $f'(v_b)$ is determined by transforming the corresponding wave functions into momentum space. The wave functions for each subshell were extracted from the Hartree-Fock code of Froese Fischer.[12]

It might be expected that the shape of the ELP is sensitively dependent on the kind of wave function of the projectile electron.[3] In order to study this dependence, ELP's were calculated with the use of Hartree-Fock (HF) wave functions[12] and scaled hydrogenic wave functions. The two sets of theoretical data differ only a little. This shows that the ELP's of the present collision systems are not particularly sensitive to the wave functions. Nevertheless, HF wave functions are used throughout the present calculations.

III. EXPERIMENTAL

The 60—200-MeV Ne^{q+} and Ar^{q+} ion beams were produced in the heavy-ion accelerator facility VICKSI at the Hahn-Meitner-Institut in Berlin. The accelerator is a combination of a 6-MV single-stage Van de Graaff accelerator and a four-sector split-pole-type cyclotron with an energy gain of a factor of 17.

The measurements were performed in a crossed-beam apparatus which has been described in more detail previously.[13] The incident ion beam of about 100 particles/nA which was focused to a diameter of 2 mm was crossed with an atomic beam target with a density times thickness product of approximately (5×10^{-3} Torr) (3 mm). Electrons emitted from the scattering region were measured by an electrostatic parallel-plate analyzer. The intrinsic resolution of the analyzer was 7.8% FWHM. The electron observation angle could be varied continuously from 18° to 160°.

It should be emphasized that special care had to be taken to avoid background caused by nuclear reactions at the high projectile energies.[14] Therefore, a beam collimation system and beam defining apertures were used at a certain distance from the entrance and exit of the target chamber. The beam stop was positioned several meters away from the target region. Quartz plates, which could be inserted in the scattering chamber and which were observed by television cameras, were used to perform the alignment and the focusing of the beam. In addition, an aperture of 2 mm could be inserted at the scattering center to control the spot size at this point. The alignment of the spectrometers with respect to the scattering center was tested with an electron gun which was mounted perpendicular to the ion beam axis at the chamber.

IV. RESULTS AND DISCUSSION

A. Energy, projectile, and charge-state dependence

The spectrum in Fig. 1 shows the structures typically observed in a secondary-electron spectrum following energetic heavy-ion—atom collisions. The maxima labeled "soft collisions" and "electron loss" are produced by electrons from the target atom and the projectile, respectively. The Auger peaks result from K-shell excitation of the projectile and the target atom. Owing to the collision kinematics, the projectile Auger peak appears twice in the spectrum at that particular observation angle. The spectrum indicates the major difficult concerning a systematic analysis of the ELP, that is, the background subtraction which is necessary to separate it from the continuous target electron distribution. We used a second-order polynomial to fit the background. A further difficulty in the

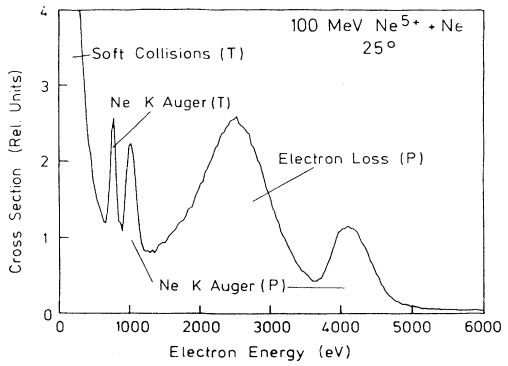

FIG. 1. Electron spectrum produced in 100-MeV $Ne^{5+}+Ne$ collisions at an observation angle of 25°. Structures originating from projectile and target atoms are labeled P and T, respectively.

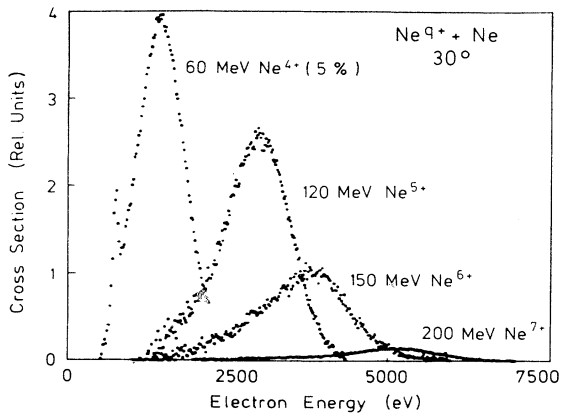

FIG. 2. Electron-loss peaks after the background subtraction from collisions with various Ne projectile ions incident on Ne.

analysis is due to structures from the target and projectile Auger electrons, which overlap with the ELP in some cases. The "binary encounter" peak[9] could cause problems due to its anisotropic angular distribution. This peak shifts towards lower electron energies with increasing observation angle and may actually be shifted through the ELP which makes a separation of the two peaks impossible for some angles.

Figure 2 shows examples of ELP's for different projectile energies and charge states. The experimental data indicate a decrease in intensity with increasing projectile energy and, in addition, a change in the shape. The answer to the question of whether these changes result from the variation of the projectile energy or from the variation of the charge state, can be given by comparison with theory as shown further below. It should be noted that the electron-emission cross sections were not measured absolutely. Therefore, in the following each experimental ELP is normalized with respect to the maximum of the corresponding theoretical curve.

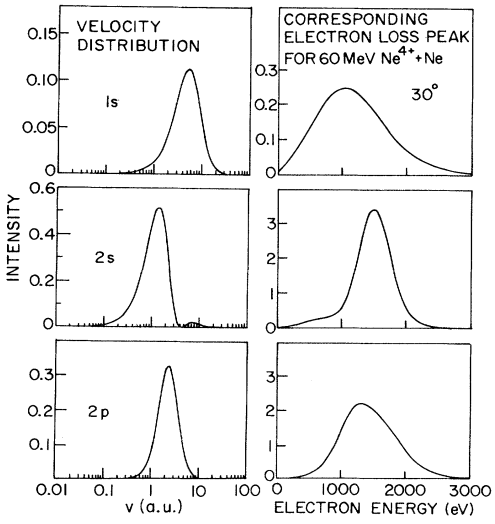

FIG. 3. Calculated ELP's or 1*s*, 2*s*, and 2*p* electrons produced in 60-MeV $Ne^{4+}+Ne$ collisions. Observation angle is 30°.

According to Eq. (1) the energy position of the ELP should be given by the projectile energy. However, this is only true if the binding energy is neglected. Actually, the center of the ELP is expected at somewhat smaller electron energies. This can be seen from Fig. 3, where calculated ELP's are plotted. For the different subshells the ELP appears at different centroid energies which depend on the initial binding of the electron. This binding energy is partially lost from the electron-emission energy. Hence, the shift of the ELP for the 1*s* electrons is understood. The nodal structure in the 2*s* wave functions produces a shoulder in the ELP. The 1*s* and 2*p* wave functions do not have a nodal structure so that the corresponding ELP's look similar. The 2*p* wave function produces a narrower and less shifted ELP, because of its smaller $\vec{v}_b'$ and smaller binding energy.

In Fig. 4 two examples are shown where the individual contributions of the 1*s* and 2*p* shell may explicitly be seen. In the case of 120-MeV Ne^{5+} the main contribution comes from the *L* shell. Since there are two electrons in the 2*s* shell, the dominant contribution to the ELP originates from this subshell. From the 2*p* shell only one electron contributes. The 1*s* electrons contribute also to the ELP. Their contribution is 15% at 30°, whereas it is about 25% for 90°. It should be noted that only relative cross sections were measured in this work. Therefore, the experimental ELP's are normalized at the maximum to the corresponding theoretical data.

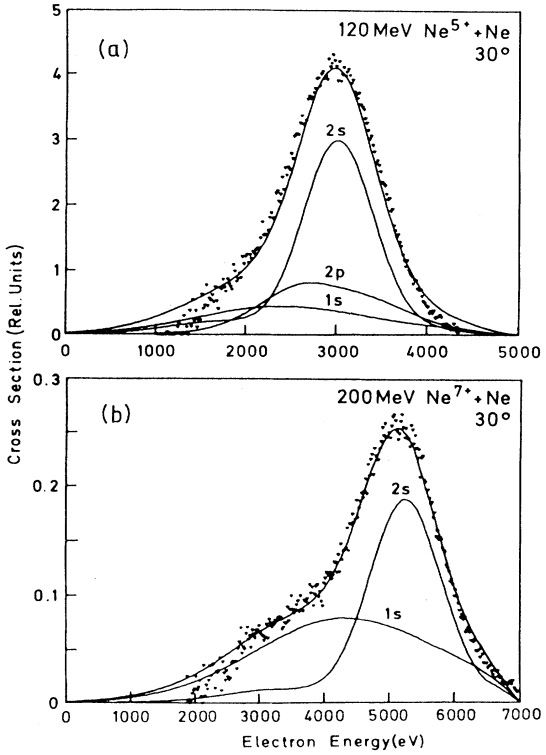

FIG. 4. Calculated ELP's for the system. (a) 120-MeV $Ne^{5+}+Ne$, (b) 200-MeV $Ne^{7+}+Ne$. Different ELP components and the sum curve are displayed. Observation angle is 30°. Experimental data are shown for comparison.

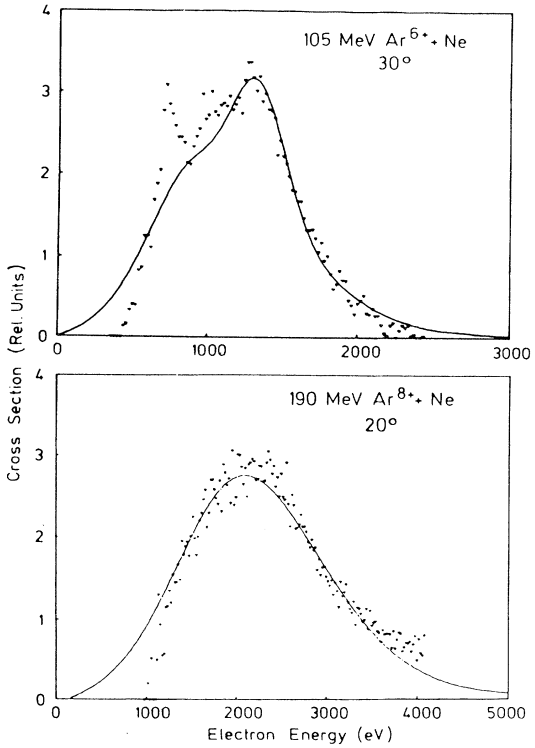

FIG. 5. Comparison of ELP's produced in collisions with 105-MeV Ar^{6+} and 190-MeV Ar^{8+} on Ne. Solid curves are calculated ELP's.

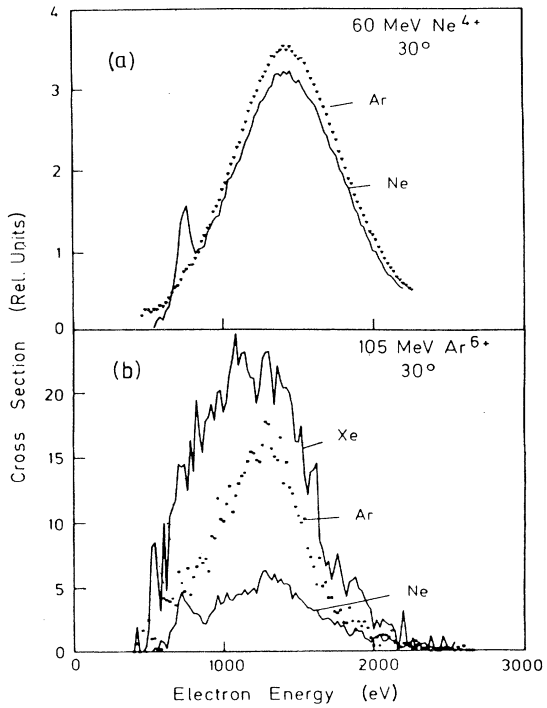

FIG. 7. Experimental ELP's observed at 30° with the use of (a) 60-MeV Ne^{4+} and (b) 105-MeV Ar^{6+} as projectiles; target gases are varied as indicated.

In the case of 200-MeV Ne^{7+} only one $2s$ electron is left. Thus, the contribution of $1s$ electrons is enhanced. However, this enhancement is not only due to the fact two $1s$ electrons are involved, it is also due to the fact that the contribution per electron increases for $1s$ electrons in relation to the $2s$ electron, as can be seen by close inspection of Fig. 4.

Figure 5 shows ELP's for 105-MeV Ar^{6+} and 190-MeV Ar^{8+} incident on Ne. In spite of the difficulties in the separation of the ELP from the background, good agreement between experiment and theory is obtained. The different shapes of the ELP's are caused by the different electronic configurations of the incident ion. In Fig. 6 experimental and calculated ELP's are compared for 105-MeV Ar^{6+}. It is noted that the left side of the ELP exhibits a peak structure due to target Ne K Auger electrons. The figure shows how much the different components contribute to the total ELP. Since the Ar^{6+} ion has only two $3s$ electrons left in the outer shells, the dominant contribution to the ELP stems from the Ar L shell. Nevertheless, the $3s$ electrons significantly influence the shape of the ELP.

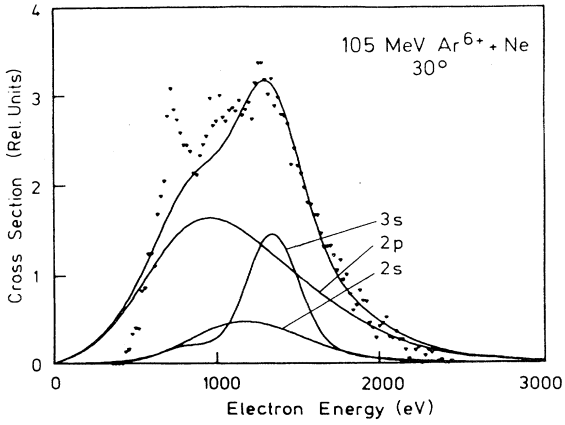

FIG. 6. Calculated ELP's for 105-MeV Ar^{6+} + Ne collisions in comparison with experimental data. Observation angle is 30°.

B. Target gas and angular dependence

The centroid energy of the ELP is independent of the target gas and the observation angle (see Sec. IV A). However, its intensity varies with the projectile charge and species for different target nuclei which are screened by their electrons. For 60-MeV Ne^{4+} on Ne and Ar and 105-MeV Ar^{6+} on Ne, Xe, and Ar the measured ELP's are plotted in Figs. 7(a) and 7(b), respectively, for a 30° observation angle. A comparison shows that the cross sections for 60-MeV Ne^{4+} and 105-MeV Ar^{6+} on Ne are very similar, but 105-MeV Ar^{6+} on Ar gives a much larger cross section for the ELP than 60-MeV Ne^{4+} on Ar.

In order to interpret the influence on the target gas, mean impact parameters and effective nuclear charges of the target atom have been estimated. The mean impact parameter $\bar{b}$ is derived from the energy transfer ΔE of the

TABLE I. Mean impact parameter $\bar{b}$ and effective target nuclear charges Z_{eff} for ionization of different atomic subshells in Ne and Ar projectiles.

Projectile	Subshell	Mean impact parameter $\bar{b}$(a.u.)	Target	Z_{eff}
60-MeV Ne^{4+}	2s	0.72	Ne	7.7
	2p	0.84	Ne	7.6
	2s	0.72	Ar	10.0
	2p	0.84	Ar	9.0
105-MeV Ar^{6+}	2s	0.30	Ne	8.2
	2p	0.40	Ne	8.0
	3s	0.78	Ne	7.7
	2s	0.30	Ar	15.2
	2p	0.40	Ar	14.1
	3p	0.78	Ar	9.5

incident nucleus to the electrons of the collision partners by the collision (in a.u.)

$$\bar{b} \approx v_p/\Delta E \ . \tag{5}$$

ΔE is determined by applying the results of Kessel *et al.*[15] and Gray and co-workers.[16] Kessel *et al.*[15] found that in 200-keV Ne^+-on-Ne collisions the additional energy transfer during the ionization of the K-shell of either the target or projectile is about the K-shell binding energy. This result can be applied to the much faster collisions investigated here. It is evident from prevoius results that the degree of multiple ionization obtained from slow Ne on Ne collisions[13] is comparable with that obtained from very fast Ne on Ne collisions.[17] This is also in agreement with Gray *et al.*[16] who measured the charge state of the recoiling Ne target. For 1-MeV/amu Ne^{6+} projectiles a projectile charge exchange from 6+ to 7+ was found. The target charge state after the collision was found to be between 3+ and 4+. It was found that the energy required to ionize the target is about the same as the energy needed to ionize the projectile. In accordance with these results it can be assumed that the energy transfer ΔE is roughly two times the binding energy E_B of the electrons lost from the projectile.

The effective nuclear charge was estimated with the use of a model recently introduced by Toburen *et al.*[18] The effective charge of the target nucleus was calculated by performing an integration of electron densities of the target up to the estimated mean impact parameter. The effective nuclear charge Z_{eff} is then the difference between the nuclear charge and the calculated electron charge fraction. The results are summarized in Table I for the different collision systems. Because the cross section $\sigma(\vec{v}_p, \vec{v}_b)$ in Eq. (4) is proportional to Z^2_{eff}, the intensity ratio of the ELP's for the different gases should be equal to the ratio of the Z^2_{eff} of these target gases. In Table II we compare the experimentally determined intensity ratios of the corresponding ELP's for Ne and Ar [see also Figs. 7(a) and 7(b)] with the corresponding ratios of the Z^2_{eff} taken from Table I. The squared target nuclear charge ratios are included in the table. It is clearly from Table II that the Z^2_{eff} ratios are in good agreement with the experimental intensity ratios. In turn, these results confirm the assumption made for the energy transfer ΔE and the mean impact parameter $\bar{b}$.

Table I shows for 60-MeV Ne^{4+} that the effective nuclear charges are about the same for the Ne and Ar target at the impact parameter of about 0.8 a.u. and the observation angle of 30°. For the Ne target the trajectory of the projectile passes the L-shell radius. Here screening is primarily produced by the K-shell electrons only. The Z^2_{eff} numbers with regard to 2s and 2p electrons are somewhat different because of the different impact parameters. For the Ar target the L-shell electrons contribute significantly to the screening. Although the nuclear charges of Ne and Ar differ by 8, the difference in the effective nuclear charges which act on the L-shell electrons of the projectile is negligible. As a result, the ELP's for both cases are about the same as seen in Fig. 7(a). The 105-MeV Ar^{6+} and 60-MeV Ne^{4+} projectiles have almost the same velocity (10.95 a.u. for Ne^{4+} and 10.15 a.u. for Ar^{6+}). Table I shows that the impact parameters which are effective for the L-shell electrons (2s,2p) in Ne and the M-shell electrons (3s) in Ar are quite similar. However, the impact parameters for the L-shell electrons in the Ar projectile

TABLE II. Experimental and theoretical intensity ratios $I_{\text{ELP}}(\text{Ar})/I_{\text{ELP}}(\text{Ne})$. Theoretical values were deduced with the use of the Z^2 scaling for the cross sections with Z_{eff} and without Z_T screening.

Projectile	$I_{\text{ELP}}(\text{Ar})/I_{\text{ELP}}(\text{Ne})$ Expt.	$I_{\text{ELP}}(\text{Ar})/I_{\text{ELP}}(\text{Ne})$ Theor. With Z_{eff}	Theor. With Z_T
60-MeV Ne^{4+}	1.1	1.5	3.2
105-MeV Ar^{6+}	3.0	3.7	3.2

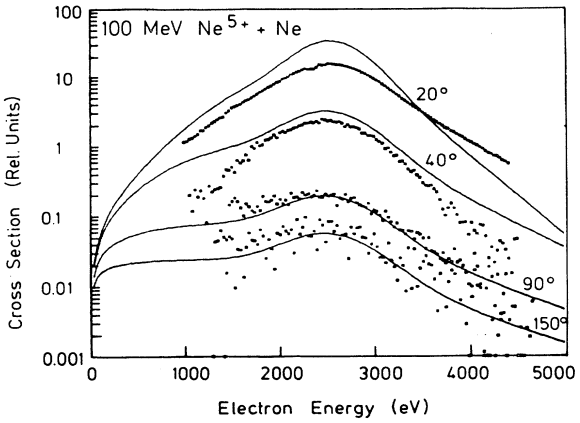

FIG. 8. Comparison of theoretical and experimental ELP's produced in 100-MeV $Ne^{5+}+Ne$ collisions. Observation angle is varied as indicated. Experimental ELP's are normalized to the calculated one for 90°.

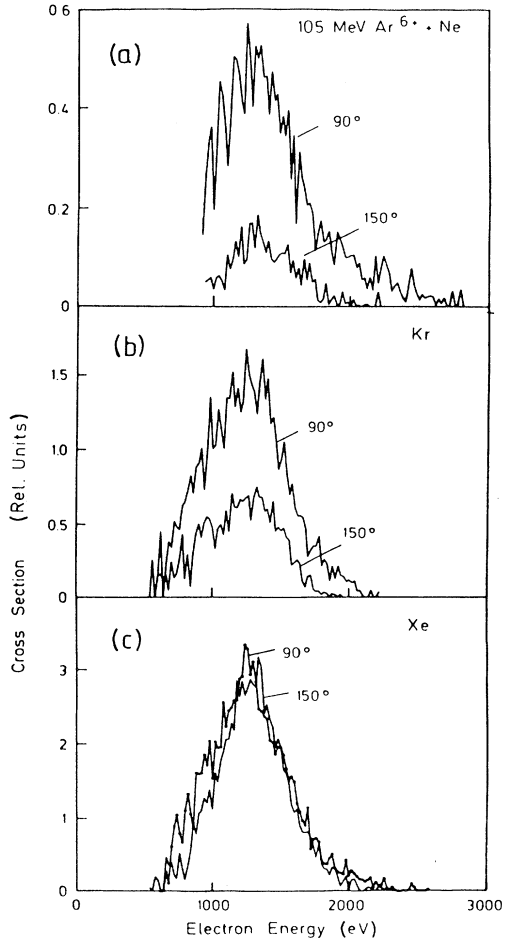

FIG. 9. Experimental ELP's observed at 90° and 150° in collisons with 105-MeV Ar^{6+}. Target gas is (a) Ne, (b) Kr, and (c) Xe.

are much smaller due to stronger binding. This means that the Ar projectile has to interpenetrate the target deeper in order to ionize its L-shell electrons. The ion therefore "feels" a larger effective nuclear charge of the target atom. Because of a lack of sufficient data which could be used to interpret the results obtained when Xe was used no interpretation is given for this case.

The influence of the target-nucleus screening may further be investigated, when the electron-observation angle is varied. In Fig. 8 experimental ELP's are compared to calculated ELP's produced in 100-MeV $Ne^{5+}+Ne$ collisions. The experimental data are normalized to the calculated ELP at 90°. The plots show that the theory overestimates the ELP for small observation angles. This is most likely due to the fact that the theory does not account for screening of the nuclear charge of the target. The data in Fig. 8 exhibit clearly the screening effects for small observation angles, i.e., glancing collision of the incident projectile electrons with the target atom. This effect should be included in further theoretical studies of the ELP.

For 105-MeV Ar^{6+} on Ne, Kr, and Xe, relative cross sections for ELP peaks were measured at observation angles of 90° and 150°. In Fig. 9 the spectra show that the cross section for the ELP at 150° increases strongly with increasing target Z compared to 90°. Again, this is mainly due to strong screening effects. Electrons at backward angles are produced in collisions with small impact parameters. Thus, if the effective nuclear charge of the target atom increases with increasing Z, the projectile electrons are ionized more effectively at a small impact parameter and hence, the cross section is increased.

V. CONCLUSION

The electron emission following the ionization of very fast Ne^{q+} and Ar^{q+} projectile ions has been measured for various combinations of projectile ions and targets. The projectile energies as high as used in the present investigation have specific advantages for the study of the electron-loss peak. The ELP appears as a pronounced maximum which may generally be well separated from the background of target electrons.

The observed electron-loss peaks have been compared in detail with theoretical results. The calculations are based on the BEA. The velocity distributions required in the analysis were deduced from Hartree-Fock calculations. The good agreement between measured and calculated ELP's allows the conclusion that the electron-loss process can be well described within the BEA for the collision systems investigated here. In particular, it is seen that inner-shell electrons contribute significantly to the ELP.

It was shown that the shape of the ELP is strongly influenced by kinematic effects. The major part of the width of the ELP can be explained by variation of the electron ejection angle in the projectile frame. Hence, it is not expected that the variation of the electron velocity adds much to the with of the ELP. As a consequence, the shape of the ELP seems to be not very sensitive on the velocity distribution and, thus, on the wave function of the bound projectile electron. This is demonstrated by the finding that the results with hydrogenic wave functions are nearly identically equal to those with Hartree-Fock

wave functions. However, the differences in the ELP's produced by $2s$ and $2p$ electrons may clearly be seen. It is evident from the comparison between measured and calculated shapes of the ELP that the theory enables a determination of the contributions of electrons from different atomic subshells.

Measurements of the angular distribution and the dependence of the ELP intensity on the target gas and on the projectile species indicate significant screening effects.

The dependence of the ELP intensity on the projectile species could be partially verified. However, the understanding of angular distributions and dependences on target gas needs further studies including screening effects of the target nucleus.

---

*Permanent address: Battelle Pacific Northwest Laboratories, Battelle Boulevard, Richland, Washington 99352.

[1]F. D. Schowengerdt, S. R. Smart, and M. E. Rudd, Phys. Rev. A 7, 560 (1973).

[2]W. E. Wilson and L. H. Toburen, Phys. Rev. A 7, 1535 (1973).

[3]D. Burch, H. Wieman, and W. B. Ingalls, Phys. Rev. Lett. 30, 823 (1973).

[4]N. Stolterfoht, D. Schneider, D. Burch, H. Wieman, and J. Risley, Phys. Rev. Lett. 33, 59 (1974).

[5]M. Breinig, M. M. Schauer, I. A. Sellin, S. B. Elson, C. R. Vane, R. S. Thoe, and M. Suter, J. Phys. B 14, L291 (1981); M. Breinig, S. B. Elston, S. Huldt, L. Lilighy, C. R. Vane, S. D. Berry, G. A. Glass, M. Schauer, I. A. Sellin, G. D. Alton, S. Datz, S. Overbring, R. Laubert, and M. Suter, Phys. Rev. A 25, 3015 (1982).

[6]F. Drepper and J. S. Briggs, J. Phys. B 9, 2063 (1976).

[7]J. S. Briggs and M. Day, J. Phys. B 13, 4797 (1980).

[8]D. H. Jakubassa, J. Phys. B 13, 2099 (1980).

[9]N. Stolterfoht, *Structures and Collisions of Ions and Atoms,* edited by I. A. Sellin (Springer, Berlin, 1978), p. 155.

[10]D. Burch, N. Stolterfoht, D. Schneider, H. Wieman, and J. S. Risley, Nuclear Physics Annual Report, University of Washington, Seattle, 1974 (unpublished).

[11]T. F. M. Bonson and L. Vriens, Physica (Ultrecht) 47, 307 (1970).

[12]C. Froese Fischer, Comput. Phys. Commun. 4, 107 (1972).

[13]N. Stolterfoht, D. Schneider, D. Burch, B. Aagaard, E. Bovin, and B. Fastrup, Phys. Rev. A 12, 1313 (1975).

[14]M. Prost, Ph.D. thesis, Hahn-Meitner-Institute, 1981 (unpublished).

[15]Q. C. Kessel, M. P. McCaughey, and E. Everhart, Phys. Rev. Lett. 16, 1189 (1966).

[16]T. J. Gray, C. L. Cocke, and E. Justiniano, Phys. Rev. A 22, 849 (1980).

[17]D. Schneider, M. Prost, B. DuBois, and N. Stolterfoht, Phys. Rev. A 25, 3102 (1982).

[18]L. H. Toburen, P. Ziem, N. Stolterfoht, D. Schneider, and M. Prost, IEEE Trans. Nucl. Sci. NS-28, 1131 (1982); L. H. Toburen, N. Stolterfoht, P. Ziem, and D. Schneider, Phys. Rev. A 24, 1741 (1981).